machines

MDPI

Article

Research on Bolt Loosening Mechanism Under Sine-on-Random Coupling Vibration Excitation

Jiangong Du, Yuanying Qiu * and Jing Li

School of Mechano-Electronic Engineering, Xidian University, Xi'an 710071, China; dujg@stu.xidian.edu.cn (J.D.); j_li@xidian.edu.cn (J.L.)

* Correspondence: yyqiu@mail.xidian.edu.cn

Abstract: This paper primarily investigates the mechanism of bolt loosening under the Sine-on-Random (SOR) vibration excitation. Firstly, a theoretical model of bolt loosening response under the SOR synthesized excitation is established by a time–frequency conversion method, which converts the sine excitation into Power Spectrum Density (PSD) expression in the frequency domain and superimposes it with random vibration excitation to obtain the SOR synthesized excitation spectrum. Then, by means of a four-bolt fastened structure, the bolt loosening mechanisms under both the sine and random vibration excitation are deeply studied, respectively. Ultimately, based on the time–frequency conversion method of SOR synthesized excitation, the bolt loosening responses of the structure under SOR excitation with different tightening torques are analyzed. Furthermore, a three-stage criterion including the Steady Stage, Transition Stage, and Loosen Stage for bolt loosening under SOR excitation is revealed, and the relationship among the SOR synthesized vibration responses and the two forms of single vibration responses is explored based on a corrective energy superposition method by introducing the weight factors of the two single vibration responses under different tightening torques. Finally, test verifications for the four-bolt fastened structure are conducted and good consistencies with the results of the Finite Element Analysis (FEA) are shown. This study provides valuable insights into the detection and prevention of loosening in bolted connection structures under multi-source vibration environments and has important engineering reference significance.

Keywords: bolt loosening; sine-on-random vibration; energy superposition method; strain monitoring; vibration test

check for updates

Academic Editors: Ciro Santus and Massimiliano De Agostinis

Received: 30 December 2024
Revised: 19 January 2025
Accepted: 21 January 2025
Published: 23 January 2025

Citation: Du, J.; Qiu, Y.; Li, J. Research on Bolt Loosening Mechanism Under Sine-on-Random Coupling Vibration Excitation. *Machines* **2025**, *13*, 80. https://doi.org/10.3390/machines13020080

Copyright: © 2025 by the authors. Licensee MDPI, Basel, Switzerland. This article is an open access article distributed under the terms and conditions of the Creative Commons Attribution (CC BY) license (https://creativecommons.org/licenses/by/4.0/).

1. Introduction

The threaded connection structure has advantages of easy installation, conciseness, small size, etc., which make it one of the most widely used and important connection methods in practical engineering [1,2]. In many megaprojects such as aerospace, railways, bridges, etc., bolt connection failure is an important factor leading to structural safety hazards and accidents. High-strength fasteners play a critical role in carrying and transmitting loads, and their failure may cause structural detachment, component loosening, and other hazards, leading to major accidents. It is of great significance to investigate the mechanism of bolt loosening under vibration [3,4].

In the last century, scholars have conducted research on the causes and theories of bolt loosening. In 1969, the German engineer Junker [5] designed a reciprocating displacement vibrostand to study the phenomenon of bolt loosening and found that the main factor of bolt loosening was transverse vibration excitation, which was widely recognized by many

scholars in recent years [6–8]. In 1978, Sakai [9] reported that when the sliding torque of the bolt head is greater than the sliding torque of the threaded surfaces, the bolt will loosen. In 1997, Zadoks [10] conducted an experiment and found that the micro slip between the clamping parts and bolts was the main cause of bolt loosening. Hess et al. [11] established a three-dimensional finite element model and provided a new method to analyze the loosening of bolts by FEA. Otter et al. [12] used different materials for bolts and connected parts and found that the influence of the structural material on bolt loosening was also obvious. Li et al. [13] proposed that bolt loosening could be categorized as either bolt head loosening or nut loosening by investigating the process of bolt loosening.

One of the important research directions is the study of different vibration excitation forms that cause bolt loosening [14]. In practical engineering, bolts are usually subjected to both sine and random vibration excitations simultaneously [15]. For example, during the running of aerospace vehicles or automobiles, the system is not only subject to periodic vibrations from the engine but also encounters random vibration sources such as environmental noise or external disturbances [16]. The superposition effect of SOR excitation may exacerbate the occurrence of bolt loosening, especially under the interaction of high-frequency sine vibration and low-frequency random vibration, making the system response more complex and the loosening process of bolts more difficult to predict. Therefore, studying the bolt loosening mechanism under SOR excitation is not only of great significance for improving the reliability and safety of structures, but is also crucial for the development of related detection and prevention technologies. Kihma et al. [17] derived a statistical rain flow cycle histogram from the SOR spectrum of the test stress data, and then used the appropriate material fatigue curve to obtain the estimated life. Cornelis et al. [18] proposed a "Mission Synthesis" method to establish the corresponding SOR power spectrum based on fatigue damage equivalence. Brown et al. [19] examined the percentile of the Cumulative Distribution Function (CDF) obtained by integrating the joint probability density functions of sine and random components. These studies provide some inspiration for the SOR vibration excitation processing method in this study.

At present, there are in-depth studies on bolt loosening under independent excitation of sine or random vibrations from multiple perspectives in the existing literature [20–23]. However, there is no research on bolt loosening under SOR vibration excitation. Currently, studies on SOR vibration are mainly focused on structural fatigue analysis. Firstly, by combining theoretical derivation and simulation analysis, the bolt loosening mechanism under SOR vibration excitation is studied by using a time–frequency conversion method. Then, a corrective energy superposition method introducing weight factors a_{T_i} and b_{T_i} is proposed, which reveals the relationship between the SOR synthesized vibration response and the individual sine or random vibration response. Finally, the effectiveness of FEA is verified through a series of vibration tests on a four-bolt fastened structure.

The summaries of the sections are as follows.

In Section 2, the relationship between SOR vibration excitation and linear system response is established, which provides a theoretical basis for investigating bolt loosening under SOR excitation.

In Section 3, for a four-bolt fastened structure model, the strain responses of monitored points of bolt loosening under sine and random vibration excitations with different tightening torques are analyzed by FEA.

In Section 4, a frequency-domain SOR vibration analysis method is proposed by synthesizing the sine vibration and random vibration excitation in Section 3, and the responses of the four-bolt structure monitored points are analyzed under SOR vibration excitation. Furthermore, the response results of monitored points under SOR synthesized excitation and independent sine and random vibration excitation are compared and analyzed, and

a relationship model of the SOR synthesized vibration response and two forms of single vibration responses based on energy superposition method is established.

In Section 5, sine and random vibration tests are conducted to verify the FEA results with the same four-bolt fastened structure. It is found that the statistical analysis of the structural test data has good consistency with that of the FEA, which proves the effectiveness of FEA and the feasibility of the proposed method.

2. Theoretical Model of System Response Under SOR Synthesized Excitation

This section establishes theoretical models for the displacement response of a Multi-Degree-of-Freedom (MDOF) system under three different vibration excitation forms. The three types of vibration excitation are sine vibration, random vibration, and SOR vibration synthesized excitation. Then, the relationship between displacement responses of MDOF and structural strain is pointed out, providing a basis for the strain-based implicit monitoring method of bolt loosening.

2.1. Displacement Response of the MDOF System Under Sine Vibration Base Excitation

Bolt loosening is evaluated through the strain responses of monitored points of the structure in this study. To achieve this, a structural theoretical model of responses under SOR vibration excitation is established.

The vibration differential equation for the MDOF system with vibration base displacement excitation is [24]

$$\mathbf{M}\ddot{\mathbf{x}} + \mathbf{C}\dot{\mathbf{x}} + \mathbf{K}\mathbf{x} = -\mathbf{M}\ddot{y}(t) \tag{1}$$

where $\mathbf{M}$ is the system mass matrix; $\mathbf{C}$ is the damping coefficient matrix; $\mathbf{K}$ is the system stiffness matrix; $\mathbf{x}$ is the displacement vector of the system; $-\mathbf{M}\ddot{y}(t)$ is the equivalent inertial force vector caused by base displacement excitation; $y(t)$ is the expression of the vibration base displacement excitation.

In practical vibration engineering such as aviation, aerospace, navigation, and vehicles, Equation (1) is often used to describe the structural vibration caused by the motion of the carrier foundation.

Supposing the base displacement excitation in sine form, it can be expressed as

$$y_{Sine}(t) = A_{Sine}\sin(\omega_{Sine}t) \tag{2}$$

where A_{Sine} is the amplitude of sinusoidal displacement excitation; $\omega_{Sine} = 2\pi f$ is the angular frequency of sine displacement excitation.

According to Equation (2), the acceleration expression of the base displacement excitation of sine vibration should be

$$a_{Sine}(t) = \ddot{y}_{Sine}(t) = -A_{Sine}\omega_{Sine}^2\sin(\omega_{Sine}t) \tag{3}$$

According to the assumption of proportional damping, the eigenvectors of the system can be solved regardless of the damping term [25]. The eigenvalue equation of Equation (1) is

$$\left(\mathbf{K} - \omega_i^2\mathbf{M}\right)\boldsymbol{\phi}_i = 0, \qquad i = 1, 2, \cdots, n \tag{4}$$

where ω_i is the i-th natural frequency of the system; $\boldsymbol{\phi}_i$ is the corresponding modal vector; n is the number of degrees of freedom.

We introduce a generalized coordinate vector $\mathbf{q}$ via coordinate transformation $\mathbf{x} = \boldsymbol{\Phi}\mathbf{q}$, where $\boldsymbol{\Phi} = [\boldsymbol{\phi}_1, \boldsymbol{\phi}_2, \ldots, \boldsymbol{\phi}_n]$ is the modal matrix of the system. By substituting Equation (4) and the generalized coordinate vector $\mathbf{q}$ into Equation (1) and left-multiplying $\boldsymbol{\Phi}^T$ into the

equation of motion, the equation of motion for each mode of the system can be written as [24]

$$\ddot{\mathbf{q}}_i + 2\zeta_i\omega_i\dot{\mathbf{q}}_i + \omega_i^2\mathbf{q}_i = -\boldsymbol{\Phi}_i^T\mathbf{M}\ddot{y}(t), \qquad i = 1, 2, \cdots, n \tag{5}$$

where ζ_i is the damping ratio of the i-th mode of the system.

For a system with zero initial conditions, according to Equations (3)–(5), its steady-state response under vibration base excitation is [26]

$$\mathbf{x} = \sum_{i=1}^{n} \boldsymbol{\Phi}_i\mathbf{q}_i = \sum_{i=1}^{n} \boldsymbol{\Phi}_i A_i \sin(\omega_{Sine}t + \varphi_i) \tag{6}$$

where the amplitude and phase are

$$\begin{cases} A_i = \frac{A_{Sine}\omega_{Sine}^2}{\sqrt{\left(\omega_i^2 - \omega_{Sine}^2\right)^2 + \left(2\zeta_i\omega_i\omega_{Sine}\right)^2}} \\ \varphi_i = \arctan\left(\frac{2\zeta_i\omega_i\omega_{Sine}}{\omega_i^2 - \omega_{Sine}^2}\right) \end{cases} \tag{7}$$

It can be observed that the displacement response of a system under only sine vibration excitation is influenced not only by the system's own properties such as natural frequency ω_i, damping ratio ζ_i, and system stiffness matrix $\mathbf{K}$, but also by the amplitude A_{Sine} and frequency ω_{Sine} of the sine excitation.

2.2. Displacement RMS Response of the MDOF System Under Random Vibration Base Excitation

For random vibration excitation, frequency-domain analysis is usually required. In Equation (5), $\ddot{y}(t)$ is the base acceleration excitation of random vibration. Assuming $\ddot{y}(t)$ is a generalized stationary process, it is described by the acceleration PSD $\mathbf{S}_{a_Rand}(\omega)$.

The frequency-domain generalized coordinate response of the system can be indicated as [27]

$$\mathbf{Q}_i(\omega) = H_i(\omega)\mathbf{S}_{a_Rand}(\omega) \tag{8}$$

where $\mathbf{Q}_i(\omega)$ is the Fourier transform of the generalized coordinate response $\mathbf{q}_i(t)$; the frequency response function is

$$H_i(\omega) = \frac{1}{\omega_i^2 - \omega^2 + j2\zeta_i\omega_i\omega} \tag{9}$$

The acceleration PSD $\mathbf{S}_{a_Rand}(\omega)$ of random vibration excitation represents the energy density of each frequency component in the frequency domain. According to Equation (8), the displacement response PSD $\mathbf{S}_{qi_Rand}(\omega)$ of generalized coordinates can be obtained [27]

$$\mathbf{S}_{qi_Rand}(\omega) = |H_i(\omega)|^2\mathbf{S}_{a_Rand}(\omega) \tag{10}$$

where the square of the modulus of $H_i(\omega)$ is

$$|H_i(\omega)|^2 = \frac{1}{\left(\omega_i^2 - \omega^2\right)^2 + \left(2\zeta_i\omega_i\omega\right)^2} \tag{11}$$

According to Equation (6), the total displacement response $\mathbf{x}$ of the system is the sum of the modal responses of each order. $\mathbf{q}_i$ is an uncorrelated random process; the total displacement response PSD $\mathbf{S}_{x_Rand}(\omega)$ is the sum of the power spectral densities of each mode [26]:

$$\mathbf{S}_{x_Rand}(\omega) = \sum_{i=1}^{n} |\boldsymbol{\Phi}_i|^2\mathbf{S}_{qi_Rand}(\omega) \tag{12}$$

The response of the system under base random excitation is random, so the statistical average energy of the system response, i.e., the RMS values, can be used to represent the response. The RMS of the displacement response **x** can be obtained by integrating and taking the root of the displacement response PSD $\mathbf{S}_{x_Rand}(\omega)$ in the frequency domain [26]:

$$RMS_{x_Rand} = \sqrt{\int_0^\infty \mathbf{S}_{x_Rand}(\omega)d\omega} \tag{13}$$

According to Equations (8)–(13), the displacement response of this system under random vibration excitation is not only related to the system's mass matrix **M**, stiffness matrix **K**, and damping ratio ζ_i, but also to the excitation PSD $\mathbf{S}_{a_Rand}(\omega)$.

2.3. Strain RMS Response of the MDOF System Under Base SOR Excitation

After theoretical analysis of the displacement response of the MDOF system under sine and random vibration excitation, respectively, its response under SOR vibration synthesized excitation could be further analyzed.

Due to the fact that the sine vibration response is solved in the time domain, while the random vibration response is solved in the frequency domain, it is rather difficult to find the relationship between the SOR vibration response and individual sine and random vibration responses. Therefore, a frequency-domain analysis method is proposed, which converts sine vibration displacement excitation in the time domain into a frequency-domain acceleration PSD expression and superimposes it with random vibration excitation PSD to obtain the acceleration PSD under the SOR synthesized excitation. The advantage of this method is that it utilizes the mode-superposition method to achieve better computational accuracy in the frequency-domain analysis of the structure.

The time–frequency conversion method used in this study assumes that the RMS value of the excitation acceleration is one of the conditions for energy equivalence, which means the frequency domain PSD acceleration RMS values match the acceleration RMS values of the sine vibration excitation in the time domain. The relationship between the sine excitation acceleration RMS and its PSD spectrum is [26]

$$RMS_{a_Sine} = \sqrt{\int_0^\infty \mathbf{S}_{a_Sine}(\omega)d\omega} \tag{14}$$

The RMS value of the acceleration of the sine excitation is called the effective value of the signal, which is $1/\sqrt{2}$ times the amplitude of the sine excitation acceleration [28]. According to Equation (3), the acceleration RMS of the sine vibration excitation is

$$RMS_{a_Sine} = \frac{A_{Sine}\omega_{Sine}^2}{\sqrt{2}} \tag{15}$$

Converting the sine vibration displacement excitation into acceleration PSD in the frequency domain, theoretically it represents a spectral value corresponding to a single frequency point in the PSD:

$$\mathbf{S}_{a_Sine}(\omega) = \frac{\left(A_{Sine}\omega_{Sine}^2\right)^2}{2}\delta(\omega - \omega_{Sine}) \tag{16}$$

where $\delta(x)$ represents the Dirac delta function [29], which is widely used to express the "Concentration" effect. It has two fundamental properties: $\delta(x)$ is zero outside of $x = 0$; $\int_{-\infty}^{\infty}\delta(x)dx = 1$. These two fundamental properties enable it to effectively express the PSD components of sine signals without considering phase.

In practical applications, it is impossible to achieve infinite excitation at a single frequency, and the spectral lines in the excitation PSD need to have continuity and integrability. Therefore, other functions need to be used to approximate the Dirac function. According to Equation (16), the trigonometric function is used to approximate the expression of sine excitation in the PSD.

$$\mathbf{S}_{a_Sine}(\omega) = \frac{\left(A_{Sine}\omega_{Sine}^2\right)^2}{2\pi\Delta f}\mathrm{tri}\left(\frac{\omega-\omega_{Sine}}{\pi\Delta f}\right) \tag{17}$$

where Δf is the bandwidth of the sine function in the PSD that approximates a triangle; the function $\mathrm{tri}(x)$ is a triangular pulse function [30], defined as

$$\mathrm{tri}(x) = \begin{cases} 1-|x|, & |x| \le 1 \\ 0, & |x| > 1 \end{cases} \tag{18}$$

at the sine excitation frequency ω_{Sine}, and the spectral line inside is an impulse triangle, while the spectral values in other frequency bands are zero.

Therefore, the sine excitation and the random excitation PSD can be superimposed in the frequency domain to solve the response of the SOR synthesized excitation PSD. According to Equations (10), (12) and (13), the displacement response RMS of the system under the SOR synthesized excitation in the frequency domain can be obtained:

$$RMS_{x_SOR} = \sqrt{\int_0^\infty \sum_{i=1}^{n} |\boldsymbol{\Phi}_i|^2 |H_i(\omega)|^2 \mathbf{S}_{a_SOR}(\omega) d\omega} \tag{19}$$

The expression of the SOR synthesized excitation in frequency-domain analysis involves a spike representing sine excitation on the basis of random vibration excitation, so the SOR synthesized excitation PSD can be expressed by

$$\mathbf{S}_{a_SOR}(\omega) = \mathbf{S}_{a_Sine}(\omega) + \mathbf{S}_{a_Rand}(\omega) \tag{20}$$

Combining Equations (19) and (20), the relationship between the displacement response RMS_{x_SOR} of the system under the SOR synthesized excitation, the displacement response $RMS_{x_Sine_PSD}$ of sine excitation in spectral conversion, and the RMS_{x_Rand} of random excitation can be obtained:

$$\begin{aligned} RMS_{x_SOR} &= \sqrt{\int_0^\infty \sum_{i=1}^{n} |\boldsymbol{\Phi}_i|^2 |H_i(\omega)|^2 \mathbf{S}_{a_SOR}(\omega) d\omega} \\ &= \sqrt{\int_0^\infty \sum_{i=1}^{n} |\boldsymbol{\Phi}_i|^2 |H_i(\omega)|^2 (\mathbf{S}_{a_Sine}(\omega) + \mathbf{S}_{a_Rand}(\omega)) d\omega} \end{aligned} \tag{21}$$

Based on the obtained displacement response under SOR vibration excitation, the strain response of the MDOF system can be solved. For the MDOF system, the strain between two points α and β can be expressed as [31]

$$\varepsilon_{\alpha\beta} = \sqrt{\varepsilon_{u_{\alpha\beta}}^2 + \varepsilon_{v_{\alpha\beta}}^2 + \varepsilon_{w_{\alpha\beta}}^2} \tag{22}$$

where $\varepsilon_{u_{\alpha\beta}}$, $\varepsilon_{v_{\alpha\beta}}$, and $\varepsilon_{w_{\alpha\beta}}$ are the components of strain between two points in the u, v, and w directions, respectively, which can be defined as

$$\begin{cases} \varepsilon_{u_{\alpha\beta}} = \frac{(u_\beta - u_\alpha) - D_{u_{\alpha\beta}}}{D_{u_{\alpha\beta}}} \\ \varepsilon_{v_{\alpha\beta}} = \frac{(v_\beta - v_\alpha) - D_{v_{\alpha\beta}}}{D_{v_{\alpha\beta}}} \\ \varepsilon_{w_{\alpha\beta}} = \frac{(w_\beta - w_\alpha) - D_{w_{\alpha\beta}}}{D_{w_{\alpha\beta}}} \end{cases} \tag{23}$$

where u, v, and w are the orthogonal displacement response components of the system response $\mathbf{x}$ at point α or β; $D_{\alpha\beta}$ is the component of the initial distance between the two points α and β in one direction among the u, v, and w directions.

The strain PSD components between two points α and β in three directions can be expressed as [32]

$$\begin{cases} \mathbf{S}_{\varepsilon_u_{\alpha\beta}}(\omega) = \frac{1}{D_{u_{\alpha\beta}}^2}\left(\mathbf{S}_{u_{\alpha\alpha}}(\omega) + \mathbf{S}_{u_{\beta\beta}}(\omega) - 2\mathrm{Re}\left\{\mathbf{S}_{u_{\alpha\beta}}(\omega)\right\}\right) \\ \mathbf{S}_{\varepsilon_v_{\alpha\beta}}(\omega) = \frac{1}{D_{v_{\alpha\beta}}^2}\left(\mathbf{S}_{v_{\alpha\alpha}}(\omega) + \mathbf{S}_{v_{\beta\beta}}(\omega) - 2\mathrm{Re}\left\{\mathbf{S}_{v_{\alpha\beta}}(\omega)\right\}\right) \\ \mathbf{S}_{\varepsilon_w_{\alpha\beta}}(\omega) = \frac{1}{D_{w_{\alpha\beta}}^2}\left(\mathbf{S}_{w_{\alpha\alpha}}(\omega) + \mathbf{S}_{w_{\beta\beta}}(\omega) - 2\mathrm{Re}\left\{\mathbf{S}_{w_{\alpha\beta}}(\omega)\right\}\right) \end{cases} \tag{24}$$

where $\mathbf{S}_{\alpha\alpha}(\omega)$ and $\mathbf{S}_{\beta\beta}(\omega)$ are the displacement response self-PSD of α and β in one direction among the u, v, and w directions, respectively; $\mathbf{S}_{\alpha\beta}(\omega)$ is the cross-PSD between α and β; $\mathrm{Re}\{\cdot\}$ represents taking the real part of the cross-PSD.

According to Equations (13), (22) and (24), the strain response RMS between points α and β is

$$\begin{aligned} RMS_{\varepsilon_{\alpha\beta}} &= \sqrt{\int_0^\infty \mathbf{S}_{\varepsilon_{\alpha\beta}}(\omega)d\omega} \\ &= \sqrt{\int_0^\infty \left(\mathbf{S}_{\varepsilon_u_{\alpha\beta}}(\omega) + \mathbf{S}_{\varepsilon_v_{\alpha\beta}}(\omega) + \mathbf{S}_{\varepsilon_w_{\alpha\beta}}(\omega)\right)d\omega} \end{aligned} \tag{25}$$

Thus, the strain response RMS values of the MDOF system under SOR synthesized excitation are obtained.

3. Analysis of Bolt Loosening Mechanism Under Sine or Random Vibration Excitation

One of the main failure modes of bolted connection structures is loosening failure, and one of the main causes of bolt loosening failure is the influence of reciprocating vibration on the structure [33]. The study of bolt loosening failure under vibration excitation is usually sine vibration at a lower frequency, while there is a lack of research on higher frequency sine vibration and random vibration excitation.

Taking a four-bolt fastened structure as an example in this paper, the strain responses of the monitored points near the bolts under sine and random vibration excitations are analyzed independently to explore the mechanism of bolt loosening in complex vibration environments.

3.1. FEA Modeling and Modal Analysis for the Four-Bolt Fastened Structure

3.1.1. FEA Modeling for the Four-Bolt Fastened Structure

The four-bolt fastened structure is modeled with the modeling software SolidWorks 2016, as shown in Figure 1, which includes a disc-shaped base with 28 M8 thread holes distributed on the inner and outer circumferences, where 12 inner holes are used to connect the base and vibrostand, and 16 outer holes are used to connect the base and fixture, which

is a special-shaped fixture composed of two plates horizontally and vertically, a rectangular clamped part, and four M10 coarse threaded bolts. The clamped part is a 10 mm thick rectangular plate, and the bolt loosening monitoring method is used to monitor the strains on the surface of the clamped part.

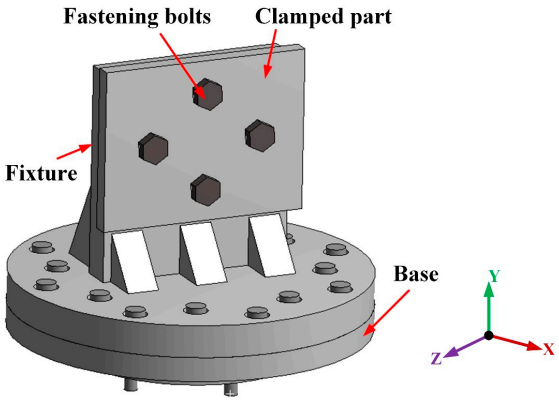


Figure 1. Model of the 4-bolt fastened structure.

In order to make the bolts and the clamped part have a more obvious difference in stiffness, carbon steel is used for the bolts and the nuts, and aluminum alloy is used for the clamped part and the fixture. The materials of the structure are shown in Table 1.

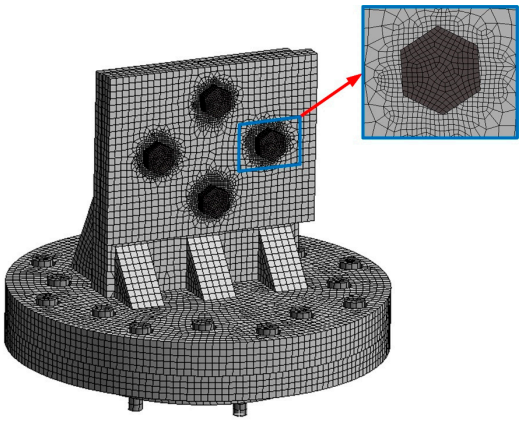
Table 1. The material information of the structure.

Components	Material	Density (kg/m^3)	Elastic Modulus (GPa)	Poisson's Ratio
Clamped part/Fixture/Base	Aluminum alloy (7075-T6)	2810	71	0.32
Bolts/Nuts	Structure steel (16MnCr5)	7800	210	0.28

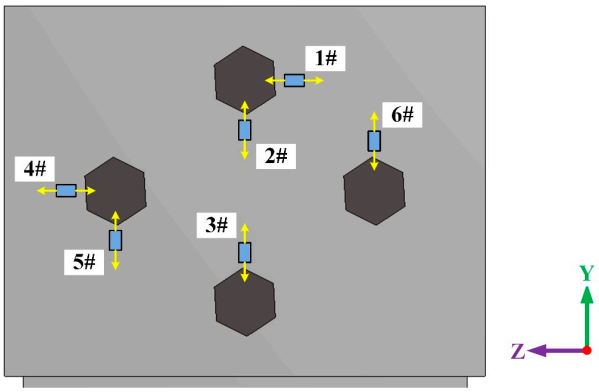
The finite element simulation software Ansys Workbench 15.0 is used to study the mechanism of bolt loosening of the four-bolt fastened structure. In modeling the FEA, the bottom of the base is set as a fixed support to simulate its connection with the vibrostand. The contact types of the following contact pairs are set as frictional type: the upper surface of the base and the bottom of the fixture; the fixture upright plate and the nut surfaces; the fixture upright plate and the contact surface of the clamped part; and the contact surface of the clamped part and the bolt heads. The frictional coefficient is set to 0.15 according to the engineering manual [34].

Multi-Point Constraints (MPCs) are used between the bolts and the nuts [35]. The MPC method is widely used for thread-region analysis in FEA. The MPC method describes the contact behavior of bolts and nuts by applying constraint relationships between their contact surfaces, which simplifies the contact problem between bolts and nuts into a coupling relationship between leader–follower nodes, without the need to establish an accurate thread model.

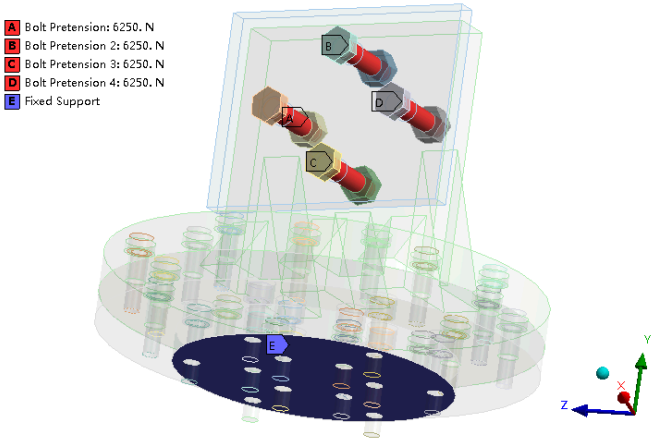
The mesh division of the FEA model is shown in Figure 2a. The global meshing type is hexahedral mesh, which has simple partitioning, high computational efficiency, and strong convergence. The global meshing element size is 4 mm, while the grid accuracy for the four fastening bolts, nuts, and their adjacent areas is refined to 1 mm to ensure the accuracy of the analysis solution.



(**a**) Model meshing of the structure



(**b**) Distribution and direction of the monitored points



(**c**) Schematic diagram of the structural load

Figure 2. Schematic diagram of the 4-bolt fastened structure.

The six monitored strain points are determined near the four bolts, with a distance of 15 mm from the center of the corresponding bolt. The monitoring direction of monitored points 1# and 4# is the Z-direction (horizontal direction), while the monitoring direction of monitored points 2#, 3#, 5#, and 6# is the Y-direction (vertical direction), as shown in Figure 2b.

Since the bottom surface of the base is connected to the vibrostand by bolts, the vibration excitation from the vibrostand is simulated by applying a Y-direction sinusoidal vibration displacement load to the bottom surface of the structure base. Figure 2c shows a schematic diagram of load application at a tightening torque of 15 N·m, where conditions A, B, C, and D represent the preload force of 6250 N applied to the four bolts, and condition E represents the surface subjected to sinusoidal vibration displacement load on the structure.

The vibration responses of the structure are analyzed under 15 different tightening torques. The following relationship exists between the bolt tightening torque T and tightening force F [34]:

$$T = KFd \tag{26}$$

where K is the torque coefficient, and $K = 0.24$ in this investigation; d is the nominal diameter of the bolts, and $d = 10$ mm in this investigation.

Equation (26) shows that for bolts with certain material and size information, the tightening force and tightening torque have a linearly positive correlation, which can be expressed by linear transformation in research. Through adjusting the tightening force successively, a set of corresponding tightening torques can be obtained.

In the FEA for this study, the finite element software Ansys Workbench 15.0 is used to exert axial force on a continuous surface cylinder (the screw surface of four bolts in this study) to achieve the corresponding bolt tightening force; 15 groups of tightening torque and their corresponding pre-tightening forces are shown in Table 2. For each analysis, a group of the same tightening torque is applied to the four bolts.

Table 2. Tightening torques of the bolts for the analysis.

Torque/N·m	3	5	7	9	11	13	15	17
Force/N	1250.0	2083.3	2916.7	3750.0	4583.3	5416.7	6250.0	7083.3
Torque/N·m	19	21	23	25	27	28.5	30	
Force/N	7916.7	8750	9583.3	10,416.7	11,250	11,875	12,500	

3.1.2. Modal Analysis for the Four-Bolt Fastened Structure

The first 20 modes of the four-bolt fastened structure are extracted for vibration excitation analysis. Different tightening torques will affect structural stiffness and natural frequency [36]; by taking the tightening torque of 15 N·m as an example, the structural nature frequencies are determined, and the first 10 orders of natural frequencies are shown in Table 3.

Table 3. The first 10 orders of natural frequencies of the 4-bolt fastened structure.

Modal Order	**1**	**2**	**3**	**4**	**5**
Natural Freq./Hz	1270.3	2504.8	2582.4	4122.1	4658.7
Modal order	**6**	**7**	**8**	**9**	**10**
Natural Freq./Hz	5172.6	5246.6	5321.9	5400.1	5882.3

According to Table 3, the first-order natural frequencies of the structure are above 1000 Hz, and only one order is below 2000 Hz, indicating that the structure has good stiffness.

3.2. Analysis of Bolt Loosening Mechanism of the Four-Bolt Fastened Structure Under Sine Vibration Excitation

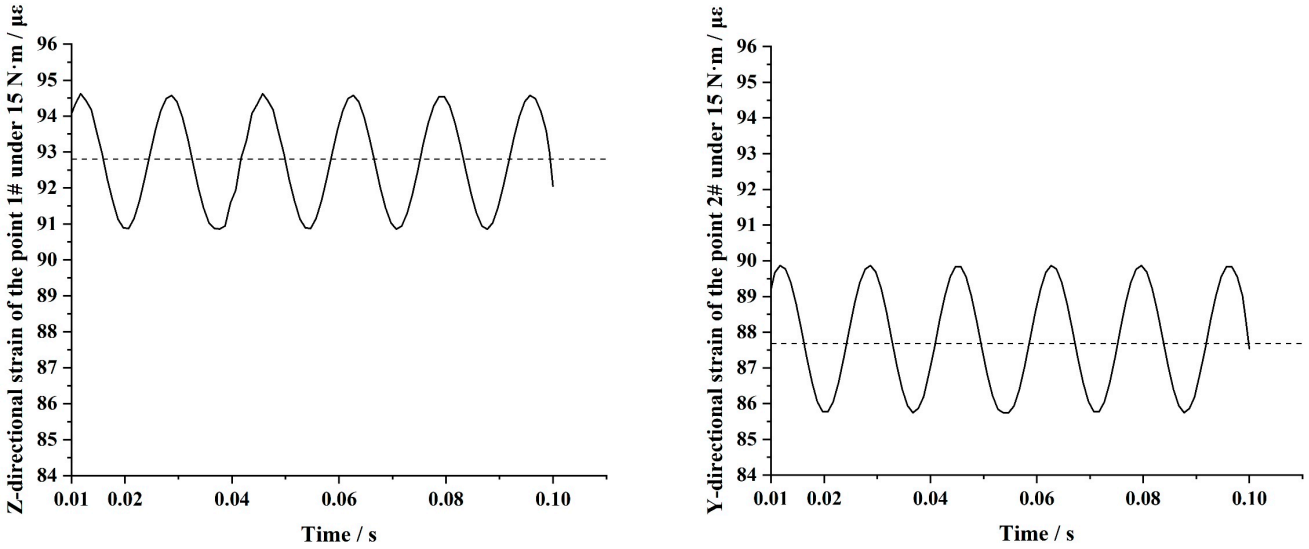
Based on the modal analysis results, the RMS strain response of the monitored bolt points in the four-bolt fastened structure under sine vibration excitation is analyzed.

The sine vibration excitation exerted to the bottom of the base in the Y-direction is given as Equation (2), supposing that the excitation amplitude A_{Sine} is 1 mm and the excitation frequency f_{Sine} is 60 Hz.

Sine vibration analyses of the structure under different tightening torques are carried out, and the strain responses of the six monitored points are obtained.

Taking the tightening torque of 15 N·m as an example, Figure 3 shows the normal strain response of monitored points 1# and 2# within 0.1 s.

As shown in Figure 3, the strain at a monitored point consists of two parts: one part is the pre-strain ε^p generated by the tightening torque and the other part is the vibration strain ε^v generated by the vibration excitation. Due to the different positions and directions, the response values of the six monitored points are different. However, their trends and patterns are the same.



(**a**) Normal strain response of 1# (**b**) Normal strain response of 2#

Figure 3. Normal strain responses of the monitored points within 0.1 s under 15 N·m tightening torque.

Since ε^p is much larger than ε^v, it is possible that ε^v would be covered up by ε^p. Thus, a workaround method is utilized in that ε^p is removed from the monitored total strain first before vibration occurring, and then only ε^v is extracted for mechanism analysis during the vibration process. It should be pointed out that ε^v is influenced not only by vibration excitation but also by the bolt tightening torque [37]; it is reasonable that ε^v can be chosen as an indicator for investigating the response of bolt loosening under the dual factors of vibration excitation and the bolt tightening torque.

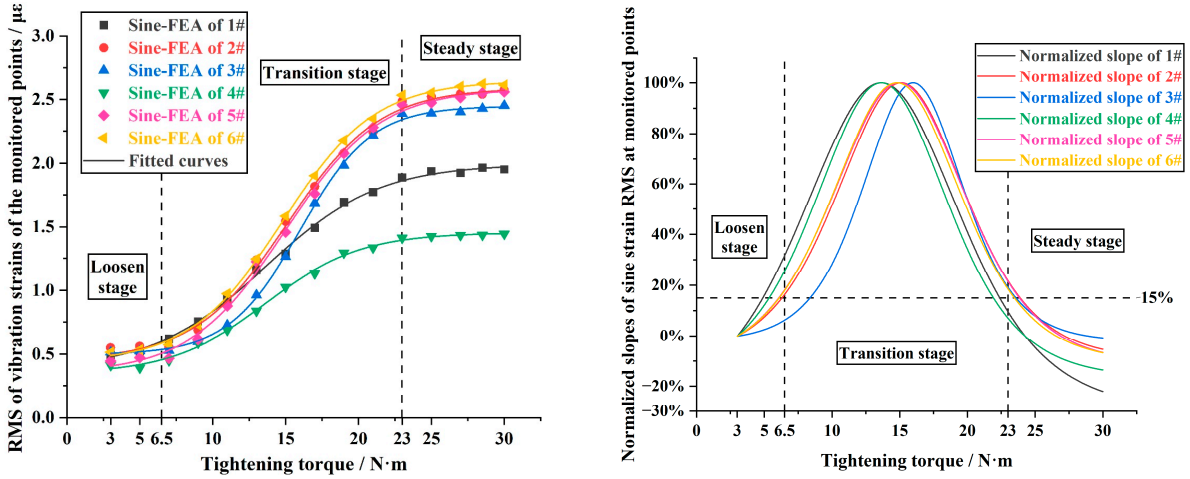
The effective value of a sine signal is called the Root Mean Square (RMS) value; the effect of vibration excitation on bolt loosening is reflected by monitoring the RMS values of vibration strains at monitored points. The following is the formula for calculating the RMS value of vibration strain at a monitored point:

$$\varepsilon^{vRMS} = \sqrt{\frac{\sum_{i=1}^{N}\left(\varepsilon^{vi}\right)^2}{N}} = \sqrt{\frac{\left(\varepsilon^{v1}\right)^2 + \left(\varepsilon^{v2}\right)^2 + \cdots + \left(\varepsilon^{vN}\right)^2}{N}} \tag{27}$$

where N donates the number of sampled strain data in the time domain; ε^{vi} is the i-th data point of the vibration strain.

The Matrix Laboratory software MATLAB R2018b is used to calculate and process the result data. The RMS values of the vibration strain response ε^{vi} at the six monitored points are shown in Figure 4a.

It can be observed that the strain RMS curves of the six monitored points are roughly divided into three stages. To quantitatively divide these three stages, we considered using the slope change rates of the strain RMS curves. However, due to the different slope ranges of the strain RMS curves at different monitored points, in order to propose a unified standard, a normalized slope method is adopted. This method normalizes the slopes of the strain RMS curves at each monitored point when the tightening torque is 3 N·m to 0%, and the maximum slope of the RMS curve within the torque ranges up to 100%. In this way, the slopes of the strain RMS curves of the six monitored points can be unified to the same slope, and by using an appropriate slope boundary as the stage division, the three stages can be quantitatively divided, as shown in Figure 4b.



(**a**) Strain RMS curves of monitored points (**b**) Normalized slopes of strain RMS curves

Figure 4. Strain RMS of FEA results varying with tightening torque under sine vibration.

From Figure 4a, it can be found that the strain ε^v RMS curves of the six monitored points have the same trend, which is because the distribution of the fastening bolts of the structure is generally symmetrical. It can be observed that the RMS values of strain responses at monitored points 1# and 4# are smaller compared to the responses of the other four monitored points. This is because the monitoring direction of monitored points 1# and 4# is the Z-direction, which is orthogonal to the vibration excitation direction of the Y-direction, while the monitoring direction of the other monitored points is the same as the excitation direction.

As shown in Figure 4b, the slopes of the strain RMS curves of the six monitored points are normalized. Using the mean tightening torque at the normalized slope of 15% for the strain RMS curves of six monitored points as the boundary torques, it can be divided into the Steady Stage, the Transition Stage, and the Loosen Stage.

For the Steady Stage, the strain RMS values always stay at a higher steady level when the tightening torque is larger than 23 N·m. This is because the bolt axial pretension remains at a high level, which ensures tightness between the bolts and fasteners.

For the Transition Stage, when the tightening torque is gradually reduced from 23 N·m to 6.5 N·m, the lower the preload, the lower the friction among the contact surfaces of the bolts and the clamped part; thus the looseness among the contact surfaces is more serious.

For the Loosen Stage, when the tightening torque is less than 6.5 N·m, the levels of strain RMS values at the six monitored points generally remain at a lower level, which means that the bolts have completely loosened and failed.

Some pivotal contact regions are assigned the frictional contact type, which is a typical nonlinear contact type and an important factor in the occurrence of nonlinear response in structures. On the other hand, the loosening mechanism of bolts is studied under vibration excitation by applying different tightening torques to bolts. The changing tightening torque is also one of the reasons for the boundary nonlinear response.

3.3. Analysis of Bolt Loosening Mechanism of the Four-Bolt Fastened Structure Under Random Vibration Excitation

Based on the mode-superposition method, the RMS strain responses of the monitored bolt points in the four-bolt fastened structure under random vibration excitation are analyzed.

In this section, a white-noise waveform acceleration PSD is applied to the bottom of the base of the structure. Figure 5 is a schematic diagram of the random vibration excitation

PSD. The frequency range of the PSD is set as 15–1000 Hz, and the spectral value is 0.2 g^2/Hz.

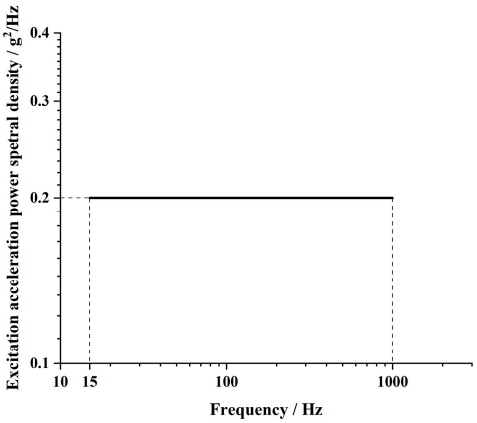
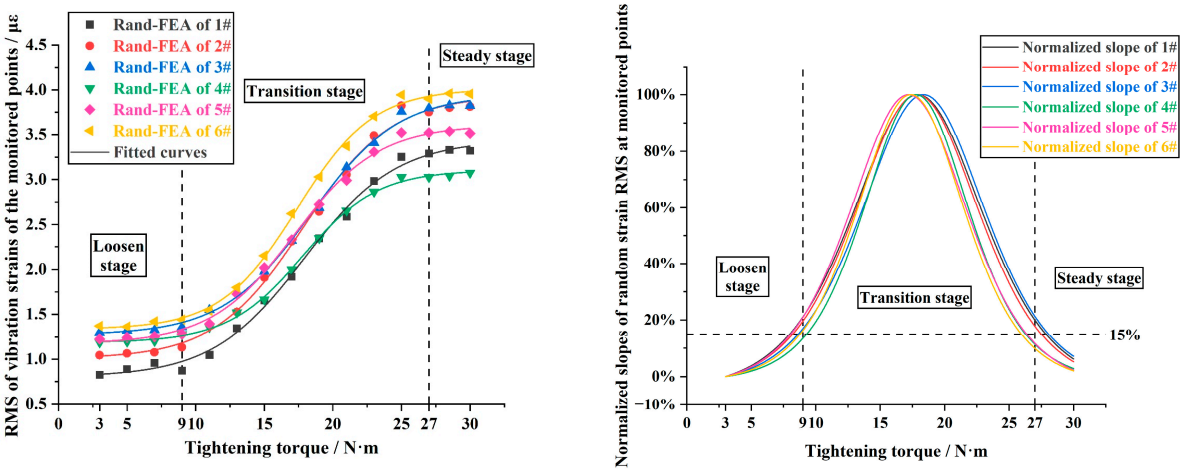


Figure 5. Random vibration excitation spectrum.

The RMS values of the strain responses of the six monitored points under random vibration with different tightening torques are extracted. Figure 6 shows the curves of the RMS values of the strain responses with varying tightening torques and the normalized slopes of the strain RMS curves.



(**a**) Strain RMS of monitored points (**b**) Normalized slopes of strain RMS curves

Figure 6. FEA strain RMS varying with tightening torques under random vibration.

It can be found that under random vibration excitation, the strain RMS values of the six monitored points have the same trend of varying with tightening torques, and the process of bolt loosening can be divided into three stages: the Steady Stage, the Transition Stage, and the Loosen Stage. This is similar to the three stages of bolt loosening under sine vibration excitation. Compared with the other four monitored points, the RMS values of the strain responses at monitored points 1# and 4# are relatively smaller because their monitoring directions are orthogonal to the excitation direction.

From Figure 6b, similarly, using a relative initial slope change of more than 15% as the boundary, the boundary tightening torques of the three loosening stages under random vibration are 27 N·m and 9 N·m, respectively, while those under sine vibration are 23 N·m and 6.5 N·m. This indicates that under random vibration, bolts will enter the Transition Stage and the Loosen Stage earlier than that under sine vibration. The reasons for this phenomenon are multifaceted. The acceleration RMS values of the two excitations are different, resulting in different bolt loosening boundaries. Considering the

energy distribution, the energy of the random vibration excitation distributes over a wide frequency range, and its upper limit is close to the structural natural frequency, while the sine vibration is only excited at a single fixed frequency of 60 Hz.

4. Investigation of Bolt Loosening Mechanism Under SOR Vibration Excitation

4.1. A Synthetic Excitation Analysis Method of SOR Vibration

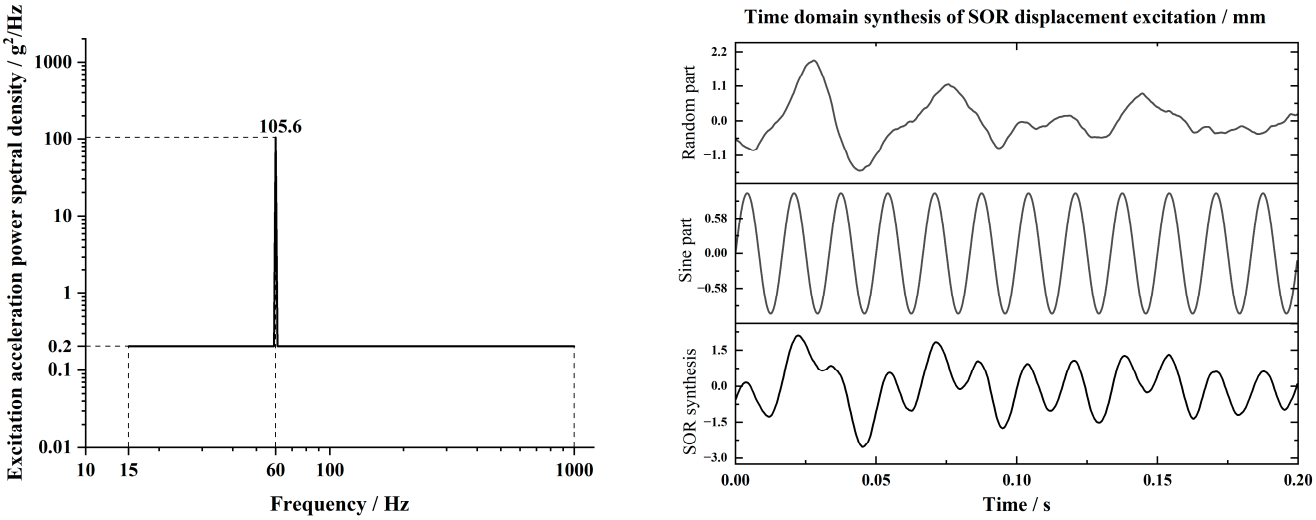
In order to analyze the effect of SOR vibration excitation on the response of bolt loosening, FEA of the strain responses of the monitored points under synthesized excitation is carried out.

A frequency-domain analysis method is proposed, which transforms sine vibration excitation into PSD expression and superimposes it with random vibration excitation PSD to obtain SOR vibration synthesized excitation PSD. The advantage of this method is that frequency-domain analysis relies on the mode-superposition method, which brings better analysis efficiency.

The excitation PSD value of sine vibration can be calculated with the excitation acceleration of the sine vibration, which can be obtained from Equation (3). Theoretically, there should be a definite spectrum value at the sine excitation frequency. However, the spectrum line of the PSD must have continuity and integrability, so it is necessary to perform spectral approximation on the PSD conversion of the sine excitation.

The meaning of PSD is the distribution function of energy in the corresponding frequency range. According to Equation (17), the frequency-domain transformation of the sine excitation is expressed approximatively as an isosceles triangle spectrum with a bottom bandwidth of only 2 Hz. The peak value of the excitation PSD can be calculated as 105.16 g^2/Hz by using the sine excitation amplitude of 1 mm and the excitation frequency of 60 Hz in Section 3.2.

To construct the synthetic excitation spectrum of the SOR vibration excitation, the sine triangle spectrum is superimposed to the white-noise excitation spectrum of the random vibration, as shown in Figure 7a, the dashed lines in Figure 7a are auxiliary lines for reading the values. The frequency-domain expression of SOR synthesized excitation PSD is not intuitive, so a more intuitive expression of SOR displacement excitation in the time domain is shown in Figure 7b.

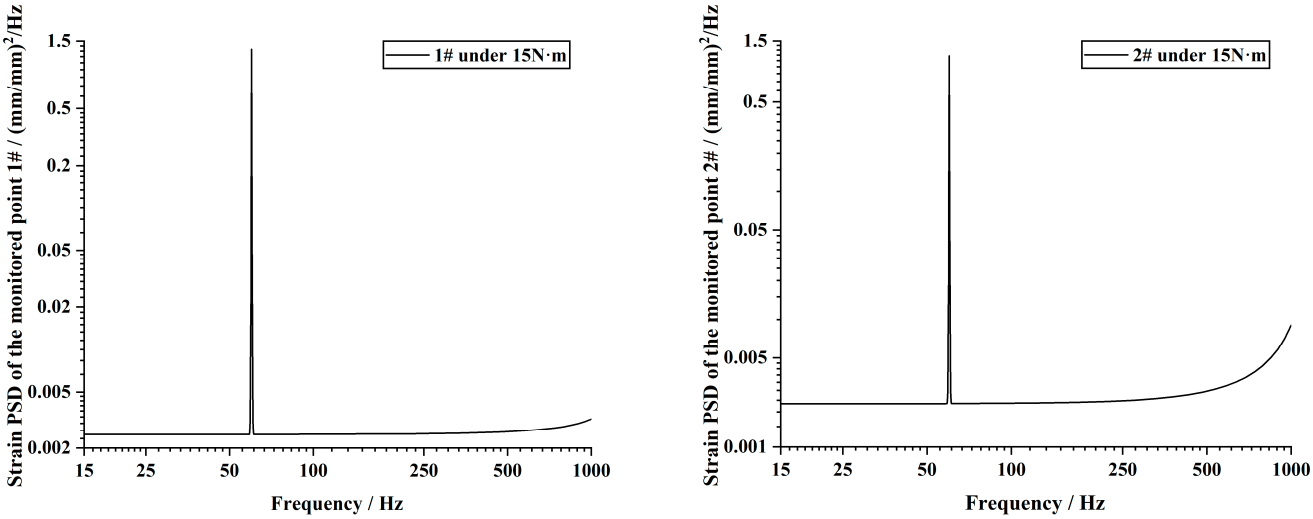


(**a**) SOR synthesize PSD in the frequency domain (**b**) SOR synthesis excitation in the time domain

Figure 7. Diagram of SOR synthesized excitation in different domains.

4.2. Response Analysis of the Monitored Points of Bolt Loosening Under SOR Vibration Excitation

Taking 15 N·m as an example, Figure 8 shows the strain response PSD of monitored points 1# and 2# under SOR synthesized excitation.

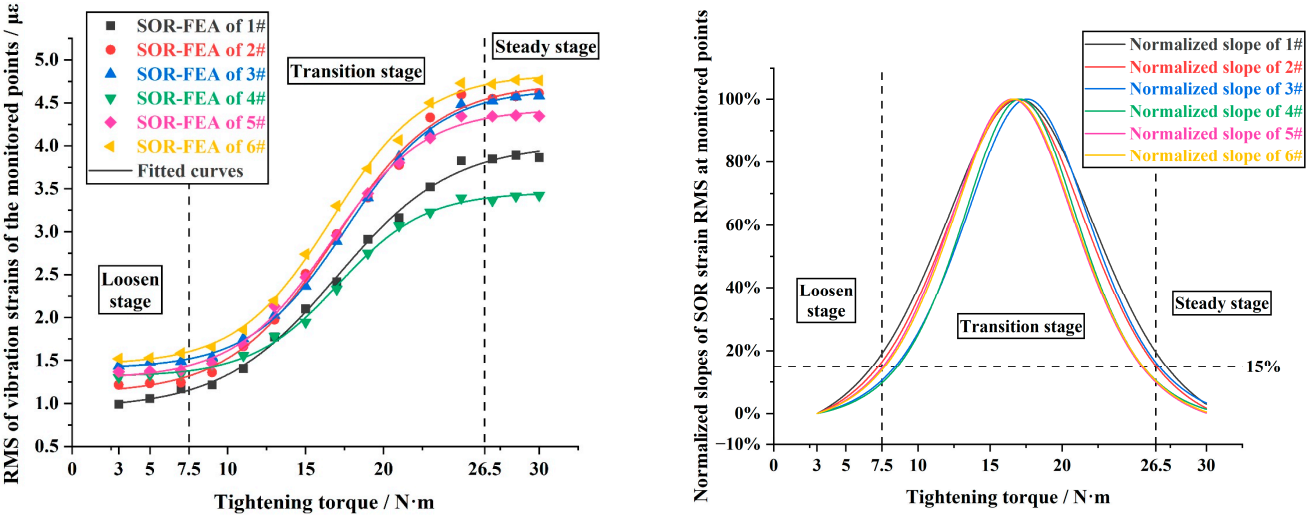


(**a**) Strain PSD of monitored point 1# (**b**) Strain PSD of monitored point 2#

Figure 8. Strain response PSD of the monitored points under SOR excitation with 15 N·m tightening torque.

It can be seen from Figure 8 that under the SOR synthesized excitation, the strain response of each monitored point only has a high peak at the sine excitation frequency of 60 Hz and maintains a stable response outside of this frequency. The response gradually increases in the latter part of the frequency range, which is because the response frequency gradually approaches the structural first-order natural frequency.

Figure 9 shows the curves of strain RMS of the six monitored points and the normalized slopes of the strain RMS curves under SOR excitation.



(**a**) Strain RMS of monitored points (**b**) RMS normalized slopes of monitored points

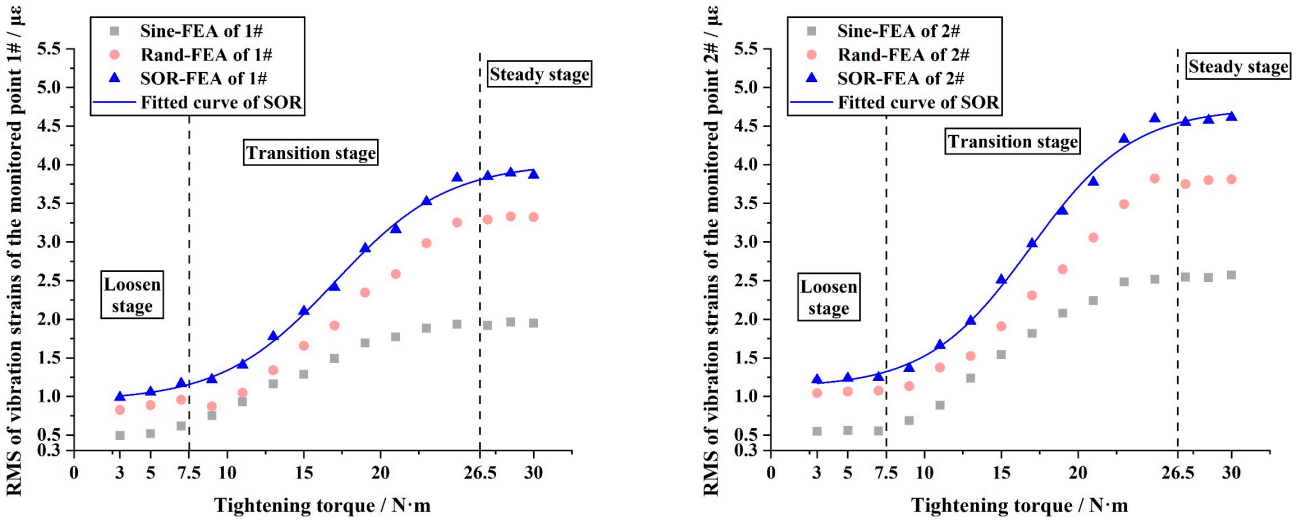
Figure 9. Curves of strain RMS of monitored points versus tightening torques under SOR synthesized excitation.

From Figure 9b, using the mean tightening torque at the normalized slope of 15% for the strain RMS curves of six monitored points as the boundary torques, which are 26.5 N·m

and 7.5 N·m, respectively, it can be divided into the Steady Stage, the Transition Stage, and the Loosen Stage.

The boundary torques of bolt loosening under SOR excitation are not the same as those under sine or random vibration excitations. When the bolts enter the Transition Stage from the Steady Stage, the boundary torque under SOR excitation is closer to the boundary torque under random excitation. And when the bolts enter the Loosen Stage from the Transition Stage, the boundary torque under SOR excitation is in the middle of the two boundary torques of the two single excitations. This indicates that under SOR excitation, random vibration dominates the bolt loosening mechanism.

Taking monitored points 1# and 2# as examples, the RMS response results of monitored points under three forms of vibration excitations are compared and analyzed, as shown in Figure 10.



(**a**) Results comparison of monitored point 1# (**b**) Results comparison of monitored point 2#

Figure 10. Comparison curves of strain RMS at monitored points under three forms of vibration.

It can be found that the strain RMS of the monitored point under SOR excitation is greater than that under single sine or random vibration excitation, but its curve trend is similar to the trends of the single vibration excitation results. Furthermore, it should be pointed out that the strain RMS values under SOR excitation are not equal to the linear superposition of that under the two single excitations.

4.3. A Relation Model Among the SOR Vibration Excitation Results and the Single Vibration Excitation Results Based on the Corrective Energy Superposition Method

In order to study the response relationship of the monitored points among SOR synthesized excitation and two forms of single vibration excitations, we take 5 N·m, 15 N·m, and 25 N·m as examples to compare their responses, as shown in Table 4.

It can be found from Table 4 that the responses under sine vibration, random vibration, and SOR vibration synthesized excitation do not simply show a linear superposition relationship. In order to investigate the nonlinear correlation among the strain RMS responses of monitored points under three forms of vibration excitations, the corrective energy superposition method (ESM) introducing weight factors is proposed, which assumes that the contributions of sine and random vibration responses to the SOR vibration response are influenced by their respective "energies".

$$RMS_{\varepsilon_SOR} = \sqrt{a_{T_i} \times RMS^2_{\varepsilon_Sine} + b_{T_i} \times RMS^2_{\varepsilon_Rand}} \quad (28)$$

where RMS_{ε_Sine} represents the vibration strain response RMS values of the time-domain sine excitation; RMS_{ε_Rand} represents the vibration strain response RMS values of the random excitation; a_{T_i} represents the energy weight factor of the sine vibration response in the SOR vibration response under the tightening torque of T_i; and b_{T_i} represents the energy weight factor of the random vibration response in the SOR vibration response under the tightening torque of T_i. It should be inferred that the weight factors a_{T_i} and b_{T_i} may be different under different tightening torques.

Table 4. RMS values of strain response of 6 monitored points under 3 forms of vibration excitation at 3 torques.

Torque (N·m)	Excitation	1# (με)	2# (με)	3# (με)	4# (με)	5# (με)	6# (με)
5	Sine	0.5211	0.5611	0.5247	0.3907	0.4721	0.5349
	Random	0.8892	1.0657	1.3179	1.1952	1.2427	1.3588
	SOR	1.0577	1.2355	1.4822	1.3345	1.3775	1.5293
15	Sine	1.2859	1.544	1.2638	1.0265	1.4577	1.5843
	Random	1.4929	1.9091	1.9775	1.6643	2.0178	2.1514
	SOR	2.1029	2.5095	2.3644	1.948	2.4711	2.7393
25	Sine	1.9372	2.5212	2.3915	1.4252	2.4753	2.5546
	Random	3.2532	3.824	3.7561	3.0278	3.5234	3.944
	SOR	3.8282	4.5956	4.4814	3.3924	4.3433	4.7294

The specific idea for obtaining the optimal weight factors a_{T_i} and b_{T_i} is shown in Figure 11.

As shown in Figure 11, for each set of tightening torques, according to Equation (28), the corresponding weight factors $a_{T_x,i,j}$ and $b_{T_x,i,j}$ can be obtained, which represent the set of weight factors obtained from the RMS responses of monitored points *i*# and *j*# under three forms of vibration excitation at the tightening torque T_x of x N·m.

Based on the weight factors $a_{T_x,i,j}$ and $b_{T_x,i,j}$, using Equation (28) with the sine vibration responses $RMS_{FEA-Sine_T_x_n\#}$ (where *n*# represents any one monitored point) and random vibration responses $RMS_{FEA-Rand_T_x_n\#}$ of the six monitored points, the theoretical SOR vibration responses $RMS_{Theo-SOR_T_x_n\#}$ of the corresponding monitored points are obtained.

Thus, the error between the theoretical calculated SOR response $RMS_{Theo-SOR_T_x_n\#}$ and the FEA SOR response $RMS_{FEA-SOR_T_x_n\#}$ of each monitored point can be obtained. There are six monitored points, so the $C_6^2 = 15$ groups of weight factors can be obtained when the tightening torque is x N·m. By introducing the Least Squares Method, the average errors between the $RMS_{Theo-SOR_T_x_n\#}$ and $RMS_{FEA-SOR_T_x_n\#}$ of the six monitored points for each set of weight factors are taken as the optimal objective function, which can obtain the optimal weight factors a_{T_x} and b_{T_x} under the tightening torque T_x of x N·m.

Finally, the same steps are carried out for responses under all groups of tightening torque, and the optimal weight factors a_{T_i} and b_{T_i} under each group of tightening torque can be obtained.

The curves of the optimal weight factors a_{T_i} and b_{T_i} under all tightening torques are shown in Figure 12.

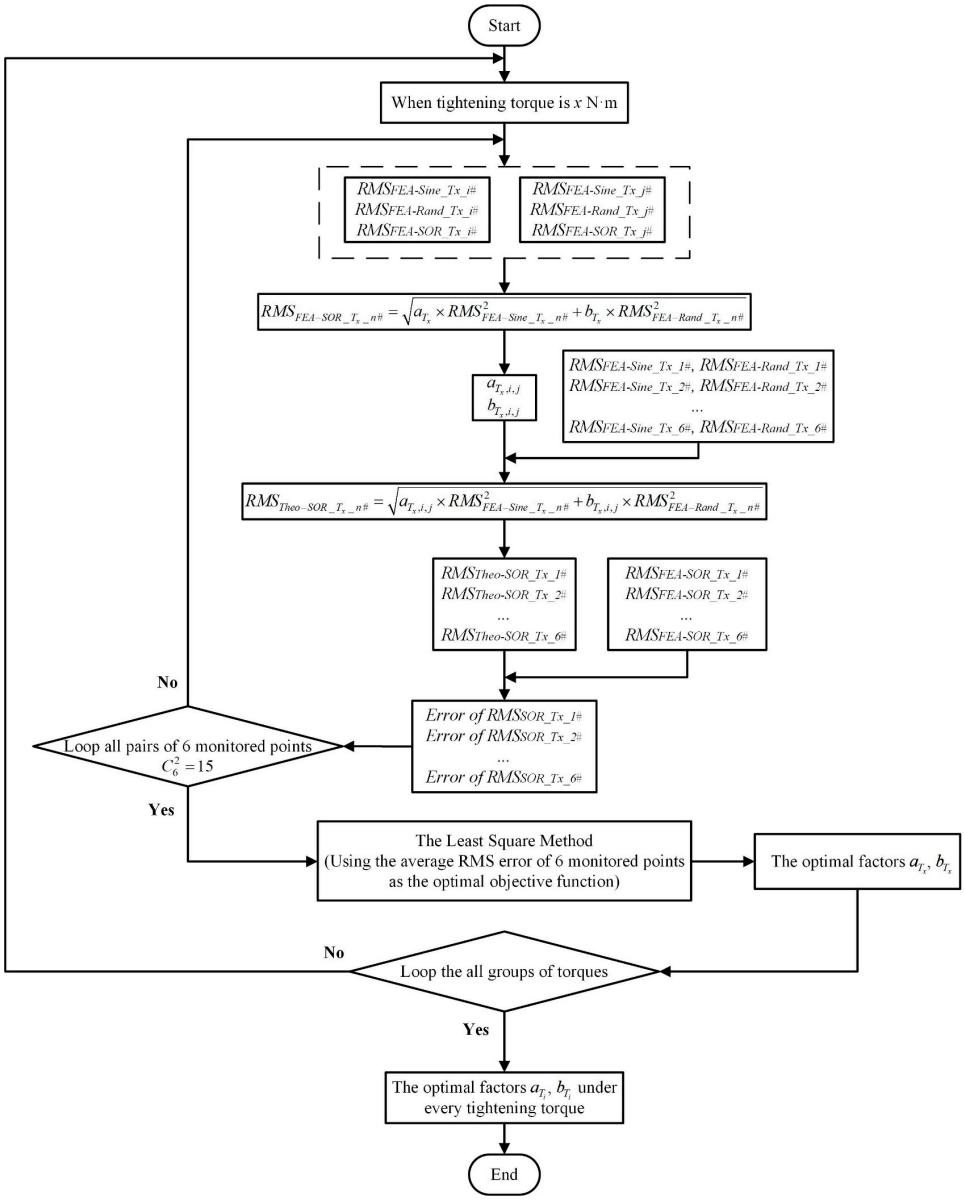


Figure 11. The calculation flowsheet for all optimal weight factors a_{T_i} and b_{T_i}.

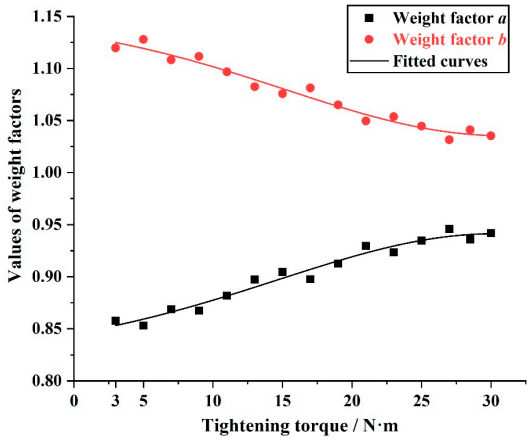


Figure 12. Curves of weight factors a_{T_i} and b_{T_i} as a function of tightening torque.

Figure 12 shows that with the increase in the tightening torques, the weight factor a_{T_i} representing the sine vibration response gradually increases, while the weight factor b_{T_i}

representing the random vibration response gradually decreases. It is also found that the weight factors a_{T_i} and b_{T_i} are basically symmetrically distributed.

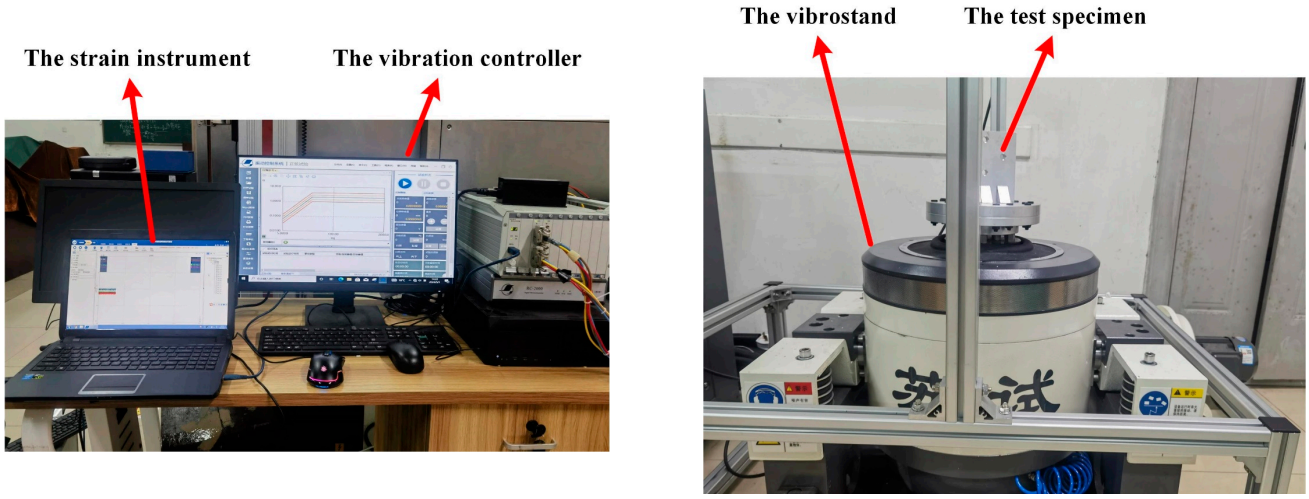
At the same time, it can be found from the numerical relationship between the weight factors a_{T_i} and b_{T_i} that, on the one hand, the factor b_{T_i} is greater than the factor a_{T_i}, which means that the random vibration response accounts for a larger proportion in the response under the SOR vibration synthesized excitation, which can also be reflected in Figure 10. On the other hand, the difference between the two weight factors gradually decreases with the increase in the tightening torques, which means that the proportions of the two forms of vibration response in the SOR synthesized vibration response gradually approach each other, because the more tight the bolts are, the less effect the vibration excitation has on the strain responses.

5. Test Verification of Bolt Loosening Detection Under Vibration Excitation

A vibration test is carried out for the four-bolt fastened structure subjected to sine vibration excitation and random vibration excitation from the vibrostand to show the agreement between the test and FEA and prove the effectiveness and feasibility of the proposed method.

5.1. Test Devices and Conditions

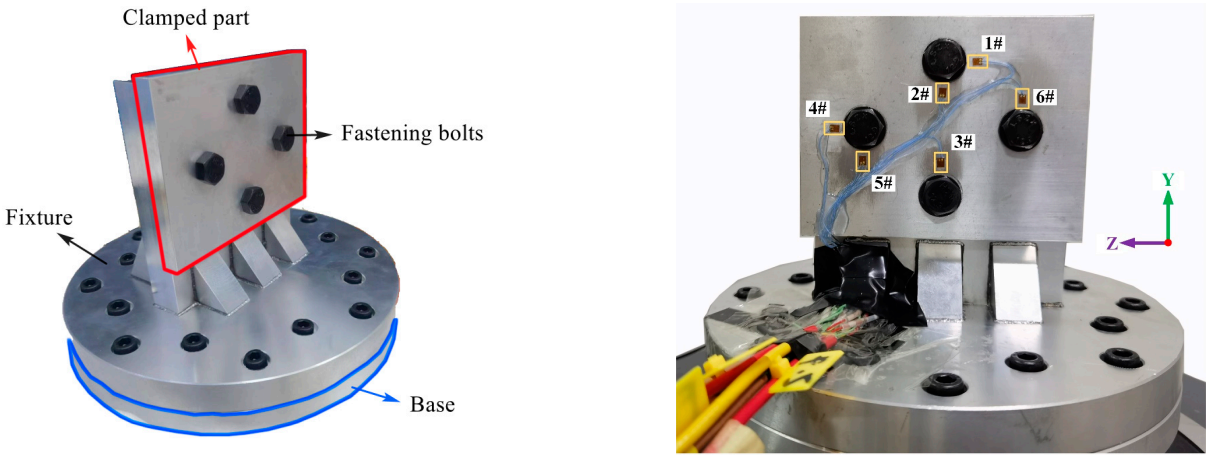
To verify the effectiveness of the loosening mechanism of the four-bolt fastened structure, a strain monitoring test for the structure under vibration is conducted. The test device including the vibration control system, the vibrostand, the test specimen, and the strain instrument is shown in Figure 13.



(**a**) The vibration controller and the strain instrument (**b**) The vibrostand and the test specimen

Figure 13. The test devices and test specimen.

The test structure, including four pairs of M10 bolts and nuts connected to 10 mm and 15 mm thick connected pieces, is shown in Figure 14. The materials and dimensions of the test structure are the same as the FEA model in Section 3.1. The base of the structure is fixed to the vibrostand by 12 bolts.



(**a**) The structure components (**b**) The distribution of the strain gauges

Figure 14. The test structure and distribution of the strain gauges.

As shown in Figure 14b, the distribution of the six monitored points 1#, 2#, 3#, 4#, 5#, and 6# on the four-bolt clamped part is consistent with that in the previous FEA. The direction of monitored points 1# and 4# is the Z-direction, and the direction of the other monitored points is the Y-direction.

A torque wrench, shown in Figure 15, is used to apply the tightening torques to the bolts, whose accuracy is 4%; 15 groups of tightening torques are applied to the bolts, as shown in Table 2. A manually preset ratchet torque wrench is utilized, with a maximum tightening torque of 50 N·m and an adjustment precision of 1 N·m per increment.



Figure 15. The torque wrench.

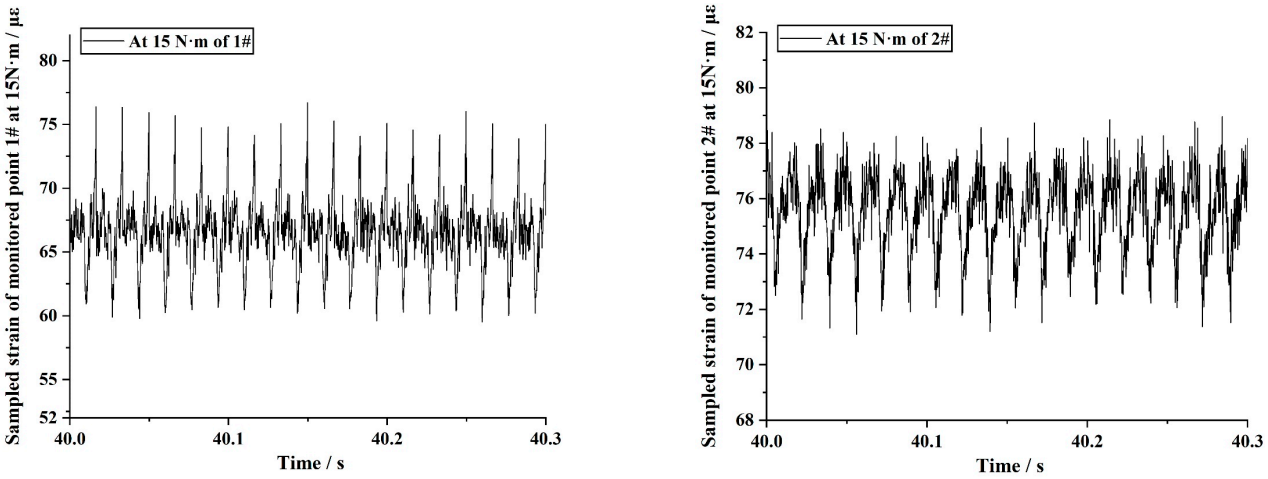
Before each group of vibration tests, the same tightening torque is applied to the four studied bolts with the torque wrench. There are 15 groups of tightening torques, as shown in Table 2 in Section 3.1. Each group of test data is sampled for 180 s. Due to the fact that the maximum frequency of random vibration excitation is 1000 Hz, to ensure that the data are not distorted and satisfy Shannon's sampling theorem [38], the sampling frequency of the strain gauge is set to 5000 Hz. To reduce the impact of random errors on the test, all of the vibration tests are conducted three times under each set of torque for the sine vibration and random vibration.

5.2. Result Analysis of the Structural Vibrations

(1) Result analysis of the structure under the sine vibration test

When conducting the sine vibration test, the excitation conditions were consistent with the FEA of the sine vibration, where the excitation amplitude was 1 mm and the excitation frequency was 60 Hz.

Taking tightening torque 15 N·m as an example, Figure 16 shows the sampled strain data of monitored points 1# and 2# from 40 to 40.3 s. There is a "warm-up period" after the vibrostand is started, during which the vibration intensity gradually increases until it reaches the target excitation parameters and remains stable. Therefore, the strain response of monitored points within the first 30 s of each group of vibration tests is not the ideal stable data. So, Figure 16 shows a section of strain response data after the vibrostand reaches stability. On the other hand, the excitation frequency for the sine vibration test conducted is 60 Hz. If a longer period of strain data is shown in the figure, it is difficult to clearly observe the strain waveform of the monitored points. When the vibrostand reaches stability, the strain data of the monitored points have the same waveform. Therefore, Figure 16 chooses to display the monitored point data within 0.3 s, which includes suitable numbers of cycles and can also show clear waveforms.



(**a**) Strain data of the monitored point 1# (**b**) Strain data of the monitored point 2#

Figure 16. Strain sampling data under sine vibration excitation with 15 N·m tightening torque.

However, it should be noted that in the subsequent data processing, this study does not use only strain data within 40 to 40.3 s, but also all valid data after the vibrostand reaches stability.

As shown in Figure 16, the sampled strain data of the monitored points include the pre-strain with the vibration strain part fluctuating on its basis. There is a slight difference in the strain mean values at different monitored points, which is caused by the fact that the two monitored points are located in different parts of the structure.

At the same time, it can be found that the sampled strain data are not a perfectly smooth sine waveform, which is due to the inevitable electromagnetic interference inside the circuit of the strain instrument. Therefore, after data sampling, it is necessary to perform filtering processing on the strain data. Through bandpass filtering of the sampled signals in the frequency band of 59–61 Hz, the strain data could be retained within the frequency band that corresponds to the sine vibration excitation frequency of 60 Hz. Furthermore, the bolt loosening stage is reflected by studying the RMS values of the vibration strains at the monitored points. Therefore, it is necessary to eliminate the pre-strain (i.e., strain mean value) generated by the tightening torque and obtain zero mean strain data. The RMS values of the strains at the monitored points can be obtained through Equation (27).

The test strain RMS values of the six monitored points varying with tightening torques are shown in Figure 17.

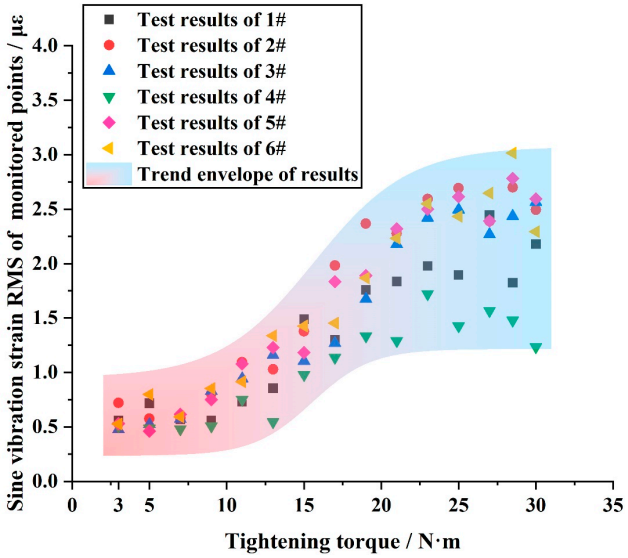
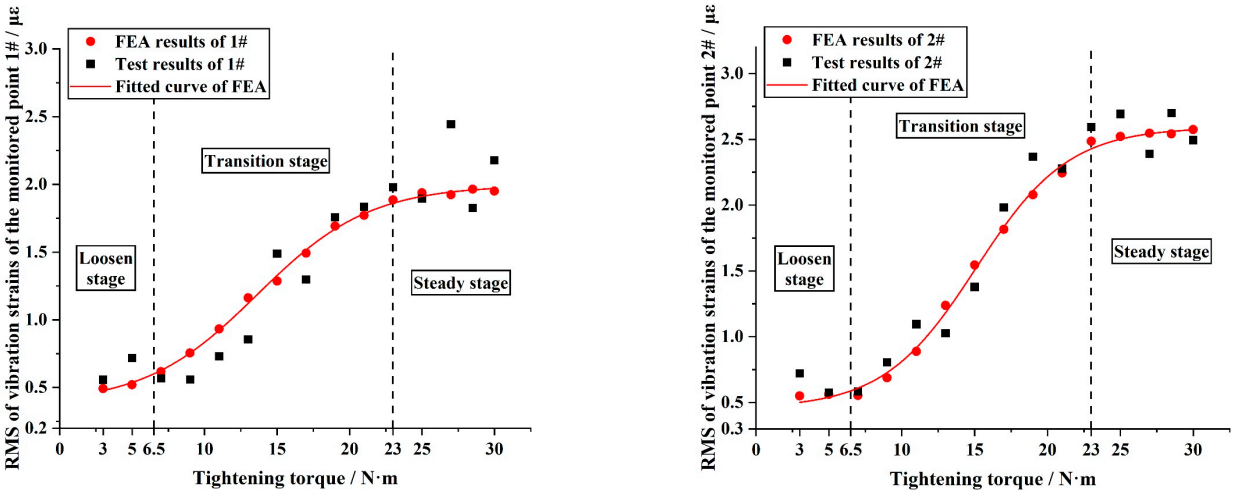


Figure 17. RMS results of strain response at the six monitored points under sine vibration test.

The approximate envelope area of the colored background in Figure 17 covers all data points. The strain RMS of monitored points 1# and 4# is smaller compared to other monitored points, because the monitoring direction of these two points is orthogonal to the excitation direction, while the others are horizontal to the excitation direction. Overall, the strain RMS of the six monitored points in the sine vibration test results showed three-stage characteristic bolt loosening.

Taking monitored points 1# and 2# as examples, a comparison between test results and FEA results under the same conditions is shown in Figure 18.



(**a**) Strain RMS comparison of 1# (**b**) Strain RMS comparison of 2#

Figure 18. Comparison between the test and FEA results of strain RMS at monitored points under sine vibration.

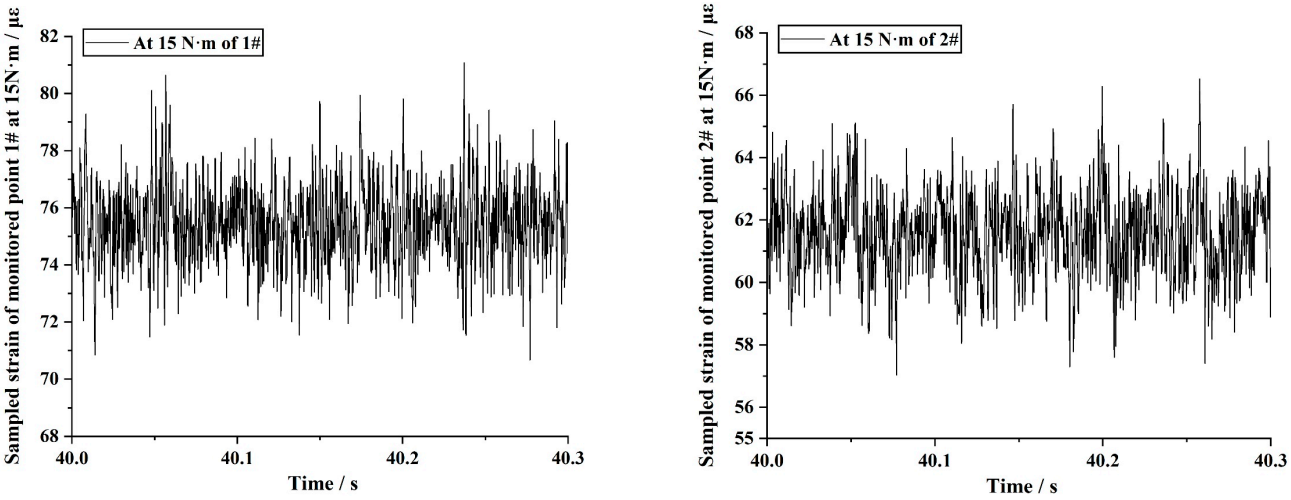
As shown in Figure 18, the black block data points represent the vibration strain RMS results of the monitored points of the sine vibration test, while the red dot data points and the fitted curves represent the FEA results under the same conditions. It can be found that the sine vibration test results are in good agreement with the FEA results, and the vibration test results can also be divided into the Steady Stage, the Transition Stage, and the Loosen Stage, which indicates the effectiveness and feasibility of both the simulation analysis method and the bolt loosening monitoring method proposed.

The average relative error between the experimental and simulation results is 8.33%. The errors between the test results and the simulation results may be caused by many factors, such as the difference between the excitation of the test vibrostand and the simulation, torque wrench error, the simplified surface contact type of the FEA model, the simulated friction coefficient, etc.

(2) Result analysis of the structure under the random vibration test

A bolt loosening test under random vibration of the structure was also conducted. The random vibration test conditions are consistent with the FEA in Section 3. The random vibration excitation is a broadband white-noise acceleration excitation PSD with a frequency range of 15–1000 Hz and a spectral value of 0.2 g^2/Hz.

Taking 15 N·m tightening torque as an example, the sampled strain data of strain gauges 1# and 2# under random vibration excitation are shown in Figure 19, with a 0.3 s duration.



(**a**) Strain data of the monitored point 1# (**b**) Strain data of the monitored point 2#

Figure 19. Strain sampling data under random vibration excitation with 15 N·m tightening torque.

It can be observed that the characteristics of sampled strain data under random vibration are not obvious. It is not possible to directly distinguish between the vibration strain data (the valid data) and the electrical noise signals (the invalid data). Therefore, it is necessary to filter the sampled strain data from the random vibration test.

The Kalman filter is a recursive linear optimal estimation method [39], suitable for handling time-varying signals and noise in dynamic systems. It can more accurately handle the dynamic changes between noise and signals. It dynamically estimates the system state and noise characteristics by assuming that the signal and noise satisfy certain statistical properties, without the need for explicit noise signal input.

The Kalman filtering method is applied to the sampled strain data, which obtains the strain data after removing the electrical noise signal. Then, the pre-strain is removed to obtain the zero mean random vibration strain responses. According to Equation (27), the RMS results of the vibration strain at the monitored points are obtained.

The test strain RMS values of the six monitored points varying with tightening torques are shown in Figure 20.

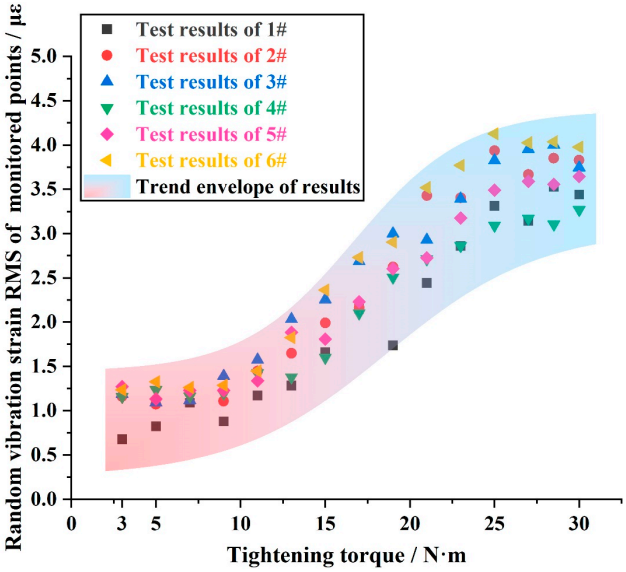
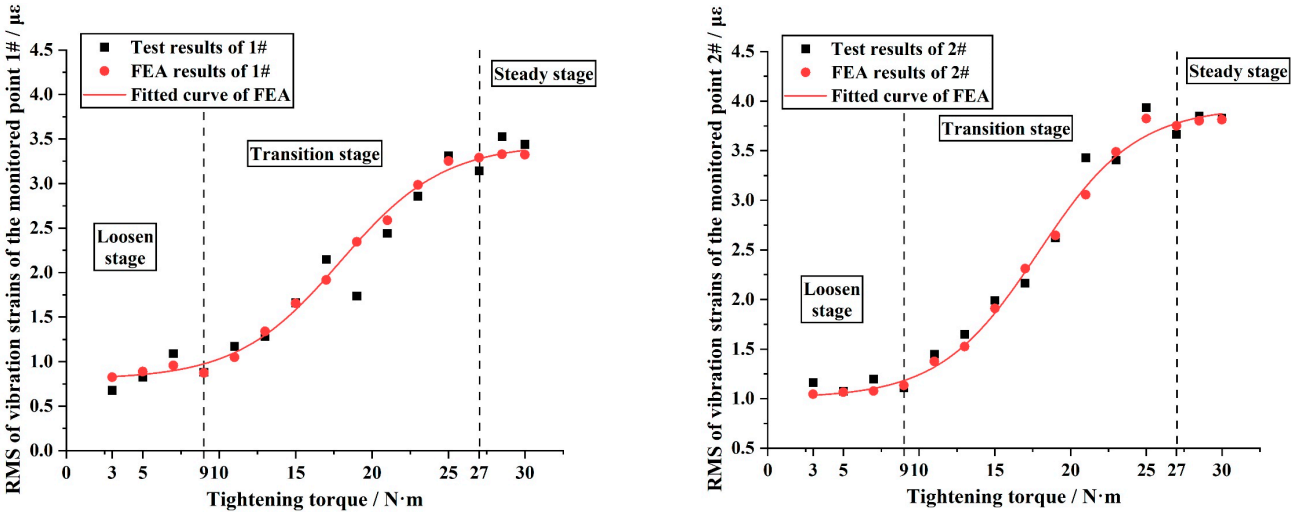


Figure 20. RMS results of strain response at the six monitored points under random vibration test.

The approximate envelope area of the colored background in Figure 20 covers all data points. The strain RMS of the six monitored points in the random vibration test results showed three-stage characteristic bolt loosening.

Taking monitored points 1# and 2# as examples, Figure 21 shows the curve of strain RMS values varying with tightening torques in the random vibration test and includes the FEA results under the same conditions.



(**a**) Strain RMS comparison of 1# (**b**) Strain RMS comparison of 2#

Figure 21. Comparison between the test and FEA results of strain RMS at monitored points under random vibration.

As shown in Figure 21, the black block data represent the test strain RMS results; the red dot data represent the FEA results. It can be observed that the test results have good consistency with the FEA results and exhibit the same trend. The curve of the RMS results of each strain gauge varying with tightening torques can be divided into three stages as well.

In summary, the vibration test results are in good agreement with the FEA results, which verifies the effectiveness of the three-stage criterion for bolt loosening under vibration excitation and the feasibility of the bolt loosening simulation analysis method proposed

herein. It also provides a reference method and ideas for bolt loosening test research for engineers or scholars in related fields.

6. Conclusions

Regarding the issue of bolt loosening under independent excitation of sine and random vibrations, some studies have conducted in-depth research from multiple perspectives. However, there is no related study on bolt loosening under Sine-on-Random vibration excitation. The bolt loosening mechanism under common Sine-on-Random vibration excitation is investigated by using a time–frequency conversion method, and the relationship between the Sine-on-Random synthesized vibration response and two forms of single sine and random vibration responses is revealed through a corrective energy superposition method with weight factors. Finally, the effectiveness of FEA is verified through the vibration tests for a four-bolt fastened structure. The main conclusions are as follows:

(a) The displacement response model of monitored points under SOR synthesized excitation is established. Based on the differential equation of motion, the response of the monitored point to sine base displacement excitation and random base acceleration PSD excitation are solved in the time domain and frequency domain, respectively. Further, by utilizing the $\mathrm{tri}(x)$ function, the sine base displacement excitation is converted as frequency-domain base acceleration excitation triangular PSD. The sine vibration and random vibration are superposed as the SOR synthesized vibration excitation according to the characteristics of the linear system. Finally, a response expression of the MDOF system under the SOR vibration synthesized excitation is deduced.

(b) The three-stage criterion for bolt loosening under SOR excitation is revealed. Through the strain RMS of the monitored points, an implicit monitoring method is used to analyze the strain response under sine, random, and synthesized excitation. It is found that there is the Steady Stage, Transition Stage, and Loosen Stage for bolt loosening.

(c) A transformed energy superposition model based on the weight factors is proposed to reflect the energy proportion of sine and random vibration responses in the SOR synthesized vibration response. In each group of tightening torque, $C_6^2 = 15$ sets of weight factors a_{T_i} and b_{T_i} can be obtained from $C_6^2 = 15$ pairs of monitored points responses under three forms of excitation (sine vibration, random vibration, and SOR synthesized vibration), where the weight factors a_{T_i} and b_{T_i} represent sine and random vibration response weights, respectively. By using the Least Square Method, the relative error between the theoretical calculated SOR response and the FEA SOR response is taken as the objective function to obtain the optimal weight factors under each group of tightening torque. Further, the influence of tightening torque on the weight factors of vibration response is studied. It can be found that there is a certain difference between the weight factors of the two forms of vibration responses when the tightening torques are small, while the weights of the two forms of vibration responses tend to be close with the increase in tightening torques. It can be found that when the bolts tend to loosen, random vibration excitation has a more significant impact on bolt loosening than sine vibration excitation, while as the bolt connections become more secure, the impacts of sine vibration and random vibration on bolt loosening are almost as much.

(d) Both sine and random vibration verification tests are conducted for a four-bolt fastened structure using a vibrostand and a specially designed clamp. The test results are highly consistent with the FEA results and reveal the approximate envelope area of the three-stage criterion for bolt loosening.

Author Contributions: Conceptualization, Y.Q. and J.L.; methodology, J.D. and Y.Q.; software, J.D.; validation, J.D., Y.Q., and J.L.; formal analysis, J.D.; investigation, J.D., Y.Q., and J.L.; resources, Y.Q. and J.L.; data curation, J.D.; writing—original draft preparation, J.D.; writing—review and editing, Y.Q. and J.L.; visualization, J.D.; supervision, Y.Q.; project administration, Y.Q. and J.L.; funding acquisition, Y.Q. and J.L. All authors have read and agreed to the published version of the manuscript.

Funding: This work is supported by the China Aerospace Science and Technology Corporation (Grant No. JSZL2017203C012), the Natural Science Basic Research Program of Shaanxi Province (Program No. 2023-JC-YB-328), and the Fundamental Research Funds for the Central Universities (Program No. ZYTS23014).

Data Availability Statement: Data are contained within the article.

Conflicts of Interest: The authors declare no conflicts of interest.

References

1. Jiang, Y.; Zhang, M.; Lee, C.-H. A study of early stage self-loosening of bolted joints. *J. Mech. Des.* **2003**, *125*, 518–526. [CrossRef]
2. Gong, H.; Liu, J.; Feng, H. Review on anti-loosening methods for threaded fasteners. *Chin. J. Aeronaut.* **2022**, *35*, 47–61. [CrossRef]
3. Huang, J.; Liu, J.; Gong, H.; Deng, X. A comprehensive review of loosening detection methods for threaded fasteners. *Mech. Syst. Signal Process.* **2022**, *168*, 108652. [CrossRef]
4. Du, J.; Qiu, Y.; Li, J. Study on the effect mechanism of vibration excitation parameters on bolt loosening based on an implicit monitoring method. *Proc. Inst. Mech. Eng. C J. Mech. Eng. Sci.* **2024**, 09544062241296930. [CrossRef]
5. Junker, G.H. New criteria for self-loosening of fasteners under vibration. *SAE Trans.* **1969**, *78*, 314–335.
6. Du, C.; Liu, J.; Gong, H.; Huang, J.; Zhang, W. Percussion-based loosening detection method for multi-bolt structure using convolutional neural network DenseNet-CBAM. *Struct. Health Monit.* **2024**, *23*, 2183–2199. [CrossRef]
7. Lin, Q.; Zhao, Y.; Sun, Q.; Chen, K. Reliability evaluation method of anti-loosening performance of bolted joints. *Mech. Syst. Signal Process.* **2022**, *162*, 108067. [CrossRef]
8. He, Z.; Shi, Z.; Qin, D.; Wen, J.; Shao, J.; Liu, X.; Xie, X. Study on Comprehensive Performance of Four-Point Contact Ball Slewing Bearings Based on a Bearing Support Bolt-Integrated Model. *Machines* **2024**, *12*, 814. [CrossRef]
9. Sakai, T. Investigations of bolt loosening mechanisms. *Bull. JSME* **1978**, *21*, 1385–1390. [CrossRef]
10. Zadoks, R.I.; Yu, X. An investigation of the self-loosening behavior of bolts under transverse vibration. *J. Sound Vib.* **1997**, *208*, 189–209. [CrossRef]
11. Pai, N.G.; Hess, D.P. Three-dimensional finite element analysis of threaded fastener loosening due to dynamic shear load. *Eng. Fail. Anal.* **2002**, *9*, 383–402. [CrossRef]
12. Otter, D.C.; Maljaars, J. Preload loss of stainless steel bolts in aluminium plated slip resistant connections. *Thin Wall. Struct.* **2020**, *157*, 106984. [CrossRef]
13. Li, Z.; Chen, Y.; Sun, W.; Jiang, P.; Pan, J.; Guan, Z. Study on self-loosening mechanism of bolted joint under rotational vibration. *Tribol. Int.* **2021**, *161*, 107074. [CrossRef]
14. Gong, H.; Ding, X.; Liu, J.; Feng, H. Review of research on loosening of threaded fasteners. *Friction* **2022**, *10*, 335–359. [CrossRef]
15. Barredo, E.; Zhao, Z.; Mazón-Valadez, C.; Larios, J.G.M.; Maldonado, I.A. A grounded inerter-based oscillating TMD for suppressing harmonic and random vibrations. *Int. J. Mech. Sci.* **2023**, *254*, 108438. [CrossRef]
16. Richards, D.; Neale, M. Effects of phase relationship in helicopter vibrations. *J. IEST* **1994**, *37*, 26–31. [CrossRef]
17. Kihm, F.; Halfpenny, A.; Ferguson, N.S. Fatigue life from sine-on-random excitations. *Procedia Eng.* **2015**, *101*, 235–242. [CrossRef]
18. Cornelis, B.; Manzato, S.; Peeters, B.; der Vorst, R.V.; Hiatt, J. A mission synthesis procedure for sine-on-random excitations in a helicopter application. In *Shock & Vibration, Aircraft/Aerospace, Energy Harvesting, Acoustics & Optics, Proceedings of the 35th IMAC, A Conference and Exposition on Structural Dynamics 2017*; Springer: Cham, Switzerland, 2017; pp. 197–209.
19. Brown, A.; McGhee, D. Statistical comparison and improvement of methods for combining random and harmonic loads. In Proceedings of the 45th AIAA/ASME/ASCE/AHS/ASC Structures, Structural Dynamics & Materials Conference, Palm Springs, CA, USA, 19–22 April 2004; p. 1535.
20. Yang, X.; Nassar, S.A. Effect of thread profile angle and geometry clearance on the loosening performance of a preloaded bolt-nut system under harmonic transverse excitation. In Proceedings of the ASME 2011 Pressure Vessels and Piping Conference, Baltimore, MD, USA, 17–21 July 2011; pp. 393–404.
21. Zheng, Z.; Huang, X.; Miao, X.; Qiu, K.; Jiang, Z.; Ding, P. Probabilistic analysis of bolted joint anti-loosening under cyclic transverse load. *Mech. Based Des. Struct. Mach.* **2024**, *52*, 7985–8011. [CrossRef]

22. Liu, G.; Zhang, L.; Han, J.; Li, M.; Su, H.; Qiao, T. Study on the influence of galloping alternating load on bolt loosening of tower. In Proceedings of the Ninth International Conference on Energy Materials and Electrical Engineering (ICEMEE 2023), Guilin, China, 25–27 August 2023; Volume 12979, pp. 895–901.
23. Dong, G.; Chen, J.; Zhao, F. Monitoring of the looseness in cargo bolts under random excitation based on vibration transmissibility. *Shock Vib.* **2021**, *2021*, 8841940. [CrossRef]
24. Geradin, M.; Rixen, D.J. *Mechanical Vibrations: Theory and Application to Structural Dynamics*, 3rd ed.; Wiley: West Sussex, UK, 2014.
25. Schmitz, T.L.; Smith, K.S. *Machining Dynamics*, 2nd ed.; Springer: Cham, Switzerland, 2019.
26. Inman, D.J. *Engineering Vibration*, 4th ed.; Pearson Education: Harlow, UK, 2014.
27. Melchers, R.E.; Beck, A.T. *Structural Reliability Analysis and Prediction*; John Wiley & Sons: Hoboken, NJ, USA, 2018.
28. Silva, C.W.d. *Vibration and Shock Handbook*, 1st ed.; CRC Press: Boca Raton, FL, USA, 2005.
29. Eftekhari, S.A. A note on mathematical treatment of the Dirac-delta function in the differential quadrature bending and forced vibration analysis of beams and rectangular plates subjected to concentrated loads. *Appl. Math. Model.* **2015**, *39*, 6223–6242. [CrossRef]
30. Wu, Z.; Lei, L.; Dong, J.; Zhang, X. Triangular-shaped pulse generation based on self-convolution of a rectangular-shaped pulse. *Opt. Lett.* **2014**, *39*, 2258–2261. [CrossRef] [PubMed]
31. Lurie, A.I.; Belyaev, A. *Theory of Elasticity*; Springer Science & Business Media: Berlin/Heidelberg, Germany, 2010.
32. Humar, J. *Dynamics of Structures*; CRC Press: Boca Raton, NJ, USA, 2012.
33. Croccolo, D.; De Agostinis, M.; Fini, S.; Mele, M.; Olmi, G.; Scapecchi, C.; Tariq, M.H. Failure of threaded connections: A literature review. *Machines* **2023**, *11*, 212. [CrossRef]
34. Childs, P. *Mechanical Design Engineering Handbook*, 2nd ed.; Butterworth-Heinemann: Oxford, UK, 2019.
35. Guzas, E.; Behan, K.; Davis, J. 3D Finite Element Modeling of Single Bolt Connections under Static and Dynamic Tension Loading. *Shock Vib.* **2015**, *2015*, 205018. [CrossRef]
36. Du, J.; Qiu, Y.; Wang, Z.; Li, J.; Wang, H.; Wang, Z.; Zhang, J. A three-stage criterion to reveal the bolt self-loosening mechanism under random vibration by strain detection. *Eng. Fail. Anal.* **2022**, *133*, 105954. [CrossRef]
37. Wang, D.; Geng, Q.; Li, Y. Effect of static load on vibro-acoustic behaviour of clamped plates with geometric imperfections. *J. Sound Vib.* **2018**, *432*, 155–172. [CrossRef]
38. Yang, Y.; Dorn, C.; Mancini, T.; Talken, Z.; Nagarajaiah, S.; Kenyon, G.; Farrar, C.; Mascareñas, D. Blind identification of full-field vibration modes of output-only structures from uniformly-sampled, possibly temporally-aliased (sub-Nyquist), video measurements. *J. Sound Vib.* **2017**, *390*, 232–256. [CrossRef]
39. Grewal, M.S.; Andrews, A.P. *Kalman Filtering: Theory and Practice Using MATLAB*, 3rd ed.; John Wiley & Sons: Hoboken, NJ, USA, 2008.

Disclaimer/Publisher's Note: The statements, opinions and data contained in all publications are solely those of the individual author(s) and contributor(s) and not of MDPI and/or the editor(s). MDPI and/or the editor(s) disclaim responsibility for any injury to people or property resulting from any ideas, methods, instructions or products referred to in the content.